V+ 2 Technical Manual Series: Neutron Dosimetry Module

December 2024

Renaissance Code Development, LLC
310 NW 5th St., Suite 203
Corvallis, Oregon 97330
(541) 286-4428
https://www.rcdsoftware.com

Preparer: Zane Tucker
DN: cn=Zane Tucker, o=Renaissance Code Development, LLC, ou=Staff Engineer, email=zane.tucker@rcdsoftware.com, c=US
Date: 2025.03.27 19:00:41 -07'00'

Reviewer: Roland R. Benke
DN: cn=Roland R. Benke, o=Renaissance Code Development, ou=General Manager, email=roland.benke@rcdsoftware.com, c=US
Date: 2025.03.28 14:20:15 -05'00'

Approver: Jeffrey Luitjens
cn=Jeffrey Luitjens, o=Renaissance Code Development, ou=Director - Software Division, email=jeff.luitjens@rcdsoftware.com, c=US
2025.03.28 14:08:16 -07'00'

ABSTRACT

VARSKIN+ (Hamby et al. 2021) is a U.S. Nuclear Regulatory Commission (NRC) computer code originally used by staff members and NRC licensees to calculate occupational dose to the skin resulting from exposure to radiation emitted from hot particles or other contamination on or near the skin. These assessments are required by Title 10 of the *Code of Federal Regulations* (10 CFR) 20.1201(c). In addition to skin contamination, NRC staff evaluate neutron dose estimates to the skin from various exposure scenarios. This document provides the V+ user with the technical basis for dosimetry calculations in the NeutronDose Module.

Table of Contents

LIST OF FIGURES

LIST OF TABLES

ACKNOWLEDGEMENTS

This report documents the work performed by Renaissance Code Development, LLC (RCD) for the U.S Nuclear Regulatory Commission (NRC) under Contract No. 31310022C0011. Staff at the Pacific Northwest National Laboratory authored initial versions of VARSKIN (US NRC 1987; US NRC 1989), with later versions amended at Colorado State University (US NRC 1992), the Center for Nuclear Waste Regulatory Analyses (US NRC 2006), and Oregon State University (US NRC 2011; US NRC 2014; US NRC 2018). RCD performed the activities described herein on behalf of the NRC Office of Nuclear Regulatory Research, Division of Systems Analysis. This report is a product of RCD and does not necessarily reflect the views or regulatory position of the NRC.

The authors are indebted to S. Bush-Goddard, B. Allen, R. Flora, J. Tomon, V. Shaffer, M. Saba, and S. Sherbini for their support during development and maintenance of many of the dosimetry models now appearing in VARSKIN+.

1.0 INTRODUCTION

NeutronDose (Figure 1-1) estimates dose to tissue at a specified depth following exposure to a source of neutrons with energies ranging several orders of magnitude from thermal to fast. The user can select monoenergetic neutrons or can choose from a list of ICRP 107 (2008) nuclides and reaction compounds resulting in various neutron spectra. Neutrons are assumed to be orthogonally incident on the body.

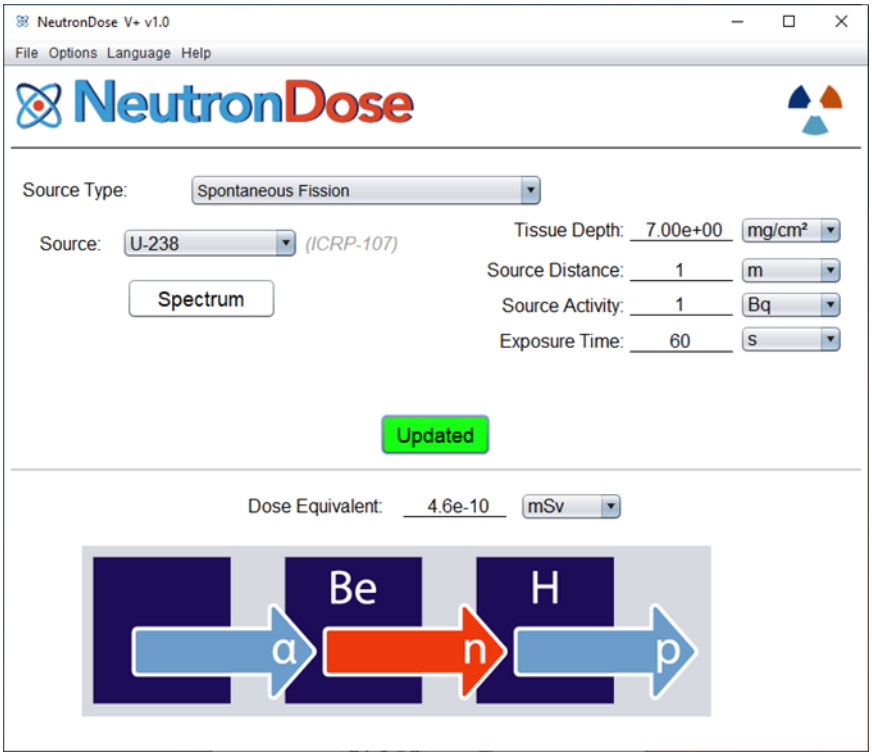

Figure 1-1. The NeutronDose User Interface

When NeutronDose is initiated, a total of six different source types are available: Spontaneous Fission; Neutron-Induced Fission; two types of Reaction source (alpha and gamma); Monoenergetic; and Custom. The first four source types (i.e., those except Monoenergetic and Custom) provide a list of pre-defined sources. The selection of Monoenergetic allows the user to enter a specific neutron energy, and Custom allows the user to upload a neutron energy spectrum. The “Spectrum” button (available for all Source Types except monoenergetic) is available to display the energy distribution of a given source.

NeutronDose contains an internal library comprised of 28 nuclides (ICRP 107 2008) which decay through spontaneous fission. The nuclides included in the library are isotopes of Cf, Cm, Es, Fm, U, and Pu. Neutron-induced fission spectra

are provided for 5 nuclides, and reaction sources are provided for 6 (α,n) and 14 (γ,n) combinations, respectively.

A custom neutron spectrum can be uploaded using a comma-delimited file with neutron energies and yields. Emission yields are normalized, if necessary. If the file provided is not a valid file (i.e., does not yield any usable data), an error dialog box will appear. An error will also be generated if an exception is generated while attempting to read the file.

2.0 NEUTRON DOSIMETRY MODEL

A new feature in VARSKIN+ is the addition of a neutron dosimetry model. Consideration is made for neutron energies ranging from 10^{-11} MeV to 20 MeV, where a set of KERMA values are generated using neutron interaction equations. The depth-dose equations can be applied to these values for an estimate of neutron dose at a specific depth in tissue. This is especially important for incident neutrons above 1 MeV because charged particle KERMA is not equivalent to dose at shallow depths. Energy degradation is halted below energies of 1 eV during scatter interactions.

This culminates in a neutron dose model in which the shallow skin dose from a monoenergetic neutron can be determined simply through the input of the neutron's energy, fluence, and tissue depth. The generalized shallow neutron dosimetry model applied in NeutronDose is:

$$H(d,E) = w_r(E) \cdot K(d,E) \cdot f_{cpe}(d,E) \qquad [2.1]$$

where $H(d,E)$ is the equivalent dose at a specific depth in tissue for a given neutron energy, relative to a perpendicular fluence of neutrons to the tissue surface. The radiation weighting factor for a given neutron at a specific energy is given by $w_r(E)$. The neutron KERMA at depth d for incident energy E is $K(d,E)$, and $f_{cpe}(d,E)$ is the depth- and energy-dependent fractional charged particle equilibrium (CPE).

2.1. Neutron Source Term

The neutron dose module provides dosimetry for six different source types: (1) spontaneous fission; (2) neutron-induced fission; (3) alpha reaction neutrons (α,n); (4) photoneutrons (γ,n); (5) a monoenergetic neutron; and (6) a user-uploaded custom energy distribution.

Spontaneous fission sources are characterized by the Watt fission spectrum:

$$\chi(E) = B_r \bar{\nu} \exp\left(-\frac{E}{A}\right) \sinh\left(\sqrt{BE}\right) \qquad [2.2]$$

Table 2-1 lists values for A and B, taken from ICRP 107 (2008) for spontaneous fission sources. The leading coefficients, B_r and $\bar{\nu}$, represent the branching ratio and average number of neutrons produced per fission for spontaneous fission events.

Table 2-1. χ(E) Data for Nuclides which Spontaneously Fission (ICRP 107)

Nuclide	Fissions/decay (B_r)	Neutrons/fission ($\bar{\nu}$)	A	B
U-238	5.45E-7	2.01	0.648	6.81
Pu-236	1.37E-9	2.13	0.998	3.10
Pu-238	1.85E-9	2.22	0.848	4.17
Pu-240	5.75E-8	2.16	0.795	4.69
Pu-242	5.54E-6	2.15	0.819	4.37
Pu-244	1.21E-3	2.30	0.695	6.00
Cm-240	3.90E-8	2.39	1.072	2.70
Cm-242	6.37E-8	2.52	0.887	3.89
Cm-244	1.37E-6	2.69	0.903	3.72
Cm-245	6.10E-9	2.87	0.912	3.62
Cm-246	2.63E-4	3.18	0.878	3.89
Cm-248	8.39E-2	3.11	0.808	4.54
Cm-250	7.40E-1	3.31	0.734	5.44
Cf-246	2.50E-6	3.10	1.026	2.93
Cf-248	2.90E-5	3.34	1.028	2.93
Cf-249	5.02E-9	3.41	1.026	2.93

Cf-250	7.70E-4	3.53	1.026	2.93
Cf-252	3.09E-2	3.77	1.025	2.93
Cf-254	9.97E-1	3.89	1.026	2.93
Es-253	8.90E-8	3.93	0.820	4.60
Es-254	3.00E-8	3.95	0.820	4.60
Es-254m	4.50E-4	3.95	0.820	4.60
Es-255	4.50E-5	3.97	0.820	4.60
Fm-252	2.30E-5	3.90	0.820	4.60
Fm-255	2.30E-7	3.73	0.820	4.60
Fm-256	9.19E-1	4.01	0.820	4.60
Fm-257	2.10E-3	3.85	0.820	4.60

For neutron-induced fission, the fission spectrum equation is modified by noting different coefficients (Table 2-2) as shown in Equation [2.3] based on a method by Walsh (1989):

$$\chi(E) = ab \exp\left(-\frac{E}{c}\right) \sinh\left(\sqrt{dE}\right) \qquad [2.3]$$

The user is further directed to Shultis and Faw (2000) and cautioned that coefficients a and b in **Error! Not a valid bookmark self-reference.** do not relate to branching ratio or neutrons per fission.

Table 2-2 χ(E) Data for Neutron-Induced Fission (Shultis & Faw 2000)

Nuclide	a	b	c	d
U-233	0.86159	0.70520	0.903	1.26

U-235	0.84180	0.65749	0.962	1.62
Pu-239	0.81547	0.70023	0.863	1.23
Th-232	0.87263	0.64188	1.030	1.83
U-238	0.86327	0.66700	0.974	1.58

Neutron dose is integrated across the energy spectrum calculated from exposure time, distance to the source, and activity of the selected spontaneous fission source. Neutron-induced fission dose is calculated based on the total neutron fluence. Additionally, distance is used only to calculate geometric attenuation of a neutron source (i.e., in a vacuum) otherwise modeled as an isotropic point.

Six alpha reaction sources can be handled by the neutron model including: AmB; AmBe; AmF; CmBe; PuBe; and PuC. Characteristics of these reactions are given in Table 2-3. Because the neutron yield per alpha is accounted for by V+, the user must specify the strength of the source in terms of the decay rate of the alpha emitter.

Table 2-3 Characteristics of V+ Alpha Reaction Sources (Lorch 1973)

Source/Target	Reaction	Avg. Neutron Energy (MeV)	Neutron yield per alpha
Am-241/B-10	$^{10}B(\alpha,n)^{13}N$	3.0	1.39E-5
Am-241/Be-9	$^{9}Be(\alpha,n)^{12}C$	4.4	7.22E-5
Am-241/F-19	$^{19}F(\alpha,n)^{22}Na$	1.5	4.17E-6
Cm-242/Be-9	$^{9}Be(\alpha,n)^{12}C$	4.1	9.17E-5
Pu-239/Be-9	$^{9}Be(\alpha,n)^{12}C$	4.6	4.70E-5
Pu-239/C-13	$^{13}C(\alpha,n)^{16}O$	4.2	3.17E-6

Alpha-reaction energy spectra were obtained from the experimental data of Anderson and Neff (1972) and Lorch (1973). The spectra can be viewed in the V+ NeutronDose module for each reaction source.

Table 2-4 lists the fourteen photoneutron sources available in V+ for neutron dosimetry. Photoneutron sources result in the emission of neutrons that are monoenergetic if the absorbed photons are monoenergetic. A small fraction of these photons may be scattered prior to absorption and therefore the neutron spectrum is said to be 'nearly' monoenergetic. The photoneutron source is modeled as purely monoenergetic in V+. As with the alpha source, neutron yield per decay is accounted for, so source strength is specified in terms of the activity of the photon emitter.

Table 2-4. Characteristics of V+ Photoneutron Sources (Shultis & Faw 2000)

Source/Target	Reaction	Avg. Neutron Energy (MeV)	Photons per decay	Neutron yield per decay*
As-76/Be-9	$^{9}Be(\gamma,n)^{8}Be$	0.108; 0.382	0.010	1.9E-6
Ga-72/Be-9	$^{9}Be(\gamma,n)^{8}Be$	0.173; 0.476; 0.733; 0.748	0.0517	1.4E-6
Ga-72/D_2O	$^{2}H(\gamma,n)^{1}H$	0.131; 0.139	0.205	1.6E-6
In-116m/Be-9	$^{9}Be(\gamma,n)^{8}Be$	0.396	0.154	2.2E-7
La-140/Be-9	$^{9}Be(\gamma,n)^{8}Be$	0.761	0.034	8.0E-8
La-140/D_2O	$^{2}H(\gamma,n)^{1}H$	0.146	0.034	2.0E-7
Mn-56/Be-9	$^{9}Be(\gamma,n)^{8}Be$	0.128; 0.397; 0.761	0.425	7.8E-7
Mn-56/D_2O	$^{2}H(\gamma,n)^{1}H$	0.146; 0.214	0.017	8.0E-8

Source/Target	Reaction	Avg. Neutron Energy (MeV)	Photons per decay	Neutron yield per decay*
Na-24/Be-9	$^{9}Be(\gamma,n)^{8}Be$	0.967	1.0	3.5E-6
Na-24/D_2O	$^{2}H(\gamma,n)^{1}H$	0.262	1.0	7.3E-6
Sb-124/Be-9	$^{9}Be(\gamma,n)^{8}Be$	0.022; 0.378	0.547	5.1E-6
Y-88/Be-9	$^{9}Be(\gamma,n)^{8}Be$	0.151; 0.949	0.999	2.7E-6
Y-88/D_2O	$^{2}H(\gamma,n)^{1}H$	0.252	0.006	8.0E-8

*neutrons emitted from 1 g of Be or D_2O placed 1 cm away.

2.2. Neutron KERMA

Neutron KERMA represents the kinetic energy transferred from neutrons to charged particles in an absorbing medium. The type and abundance of reactions that could occur depends on the incident neutron energy, elemental composition of tissue, and the various reaction cross sections as specified in Eq. [2.4]:

$$K(d,E) = \sum_j N_j \sum_i \epsilon_{ij}(E) \cdot \sigma_{ij}(E) \cdot \Phi(d,E) \qquad [2.4]$$

where N_j is the number of atoms per unit mass of element j defined by the ICRU 44 (1989) elemental composition of soft tissue (Table 2-5), $\epsilon_{ij}(E)$ is the energy transferred to charged particles as kinetic for nuclide j and interaction i, and $\sigma_{ij}(E)$ is the microscopic cross section for a given reaction. The neutron fluence (Eq. [2.5]) after attenuation through thickness d of tissue is:

$$\Phi(d,E) = \Phi(E) \cdot e^{-\Sigma_t d} \qquad [2.5]$$

The total macroscopic cross section (Σ_t) describes the probability of any interaction within that medium and can be calculated by Eq. [2.6]:

$$\Sigma_t(cm^{-1}) = \sum_i N_i \cdot \sigma_{elastic} + N_i \cdot \sigma_{inelastic} + N_i \cdot \sigma_{capture} + N_i \cdot \sigma_{transfer} \quad [2.6]$$

Unlike KERMA, absorbed dose requires consideration of energy transferred specifically to ionization by secondary charged particles within the dose volume. However, these two values are closely related such that determination of KERMA can be used to approximate dose, with the appropriate application of fractional CPE when they are not equal.

Table 2-5. ICRU (1989) Composition of Soft Tissue

Element, i	Mass Fraction	N_j (atoms/kg)
Hydrogen	0.1012	6.093×10^{25}
Carbon	0.1110	5.570×10^{24}
Nitrogen	0.0260	1.118×10^{24}
Oxygen	0.7618	2.867×10^{25}

2.3. Fractional Charged Particle Equilibrium (f_{cpe})

Neutron KERMA is equivalent to dose where CPE is established. In small incremental volumes of tissue, CPE is said to exist if every charged particle leaving the volume is replaced by a charged particle entering with the same energy. Before this, at shallower depths in tissue, charged particle equilibrium does not occur. This region is known as the buildup region, where each subsequent volume of interest approaches equilibrium. Dose is equivalent to KERMA at the depth where CPE is established. Fractional CPE represents the fraction of KERMA contributing to dose at a particular depth in the buildup region for a given incident neutron energy. This fraction is necessary to evaluate absorbed dose at shallow depths.

For neutrons incident on tissue, the primary contributor to KERMA is an elastically scattered hydrogen atom because of its large cross section and relatively high abundance. An elastically scattered hydrogen nucleus (proton) can have a maximum energy equivalent to the incident neutron energy. As such, CPE occurs at the maximum range of a proton in tissue with kinetic energy equal to the incident

neutron energy. When separate tabulated conversions from neutron fluence to dose assume CPE exists for all incident neutron energies, these tabulations become inaccurate for critical skin depths, such as those necessary to estimate shallow neutron dose. For incident neutron energies greater than about 2 MeV, the maximum range of the recoil proton exceeds the 0.007 cm depth at which shallow dose is determined. Absorbed dose for energies greater than 2 MeV, therefore, is only a fraction of KERMA at the shallow depth. For relatively short-range recoil protons (< 350 microns) from incident neutrons less than 5 MeV, tissue segments were simulated at thicknesses of 5 microns. The following function was developed from the MCNP results and is applicable for neutron energies between 1 and 5 MeV:

$$f_{cpe}(E,\ell) = A + 10B\ell + 10C\ell\ln(10\ell) \quad [2.7]$$

where ℓ is the tissue depth of interest in centimeters and A, B, and C are energy dependent coefficients for neutron energy in MeV determined from respective fits:

$$A = aE^4 + bE^3 + cE^2 + dE + e \quad [2.8]$$

$$B = a + bE^{0.5} + cE + dE^{1.5} + eE^2 + fE^{2.5} + gE^3 + hE^{3.5} \quad [2.9]$$

$$C = a + \frac{b}{E^{1.5}} + \frac{c\ln(E)}{E^2} + \frac{d}{E^2} \quad [2.10]$$

Table 2-6 lists the coefficients a through h.

Table 2-6. Coefficients for evaluating Eq. [2.8], [2.9], and [2.10] with neutron energies between 1 and 5 MeV

	A [2.8]	B [2.9]	C [2.10]
a	-0.0011	28750.5170	-2.977
b	0.0085	-129230.7936	233.4216
c	-0.0121	243025.4594	-146.5497
d	-0.0318	-249298.7577	-259.5103

e	0.1959	151141.5442	
f		-54262.00968	
g		10695.8419	
h		-893.8685	

For incident neutrons from 5 to 20 MeV, the maximum recoil range of protons is enough to allow for tissue segmentation of 10 microns. The resulting functional fit to the MCNP data is given as:

$$f_{cpe}(E,\ell) = A + B\ell + C\ell^2 + D\ell^3 \qquad [2.11]$$

again, where the tissue depth, ℓ, is given in units of centimeters and A, B, C, and D are energy dependent coefficients described by:

$$A = aE^4 + bE^3 + cE^2 + dE + e \qquad [2.12]$$

$$B = a + bE^{1.5} + cE^3 + d\ \ln(E) \qquad [2.13]$$

$$C = a + bE^2\ln(E) + c\ \ln(E) + \frac{d}{E^2} \qquad [2.14]$$

$$D = a + \frac{b}{E} + \frac{c}{E^2} + \frac{d}{E^3} \qquad [2.15]$$

The energy of incident neutron, E, is expected in units of MeV. Table 2-7 shows the respective coefficients for these equations.

Table 2-7. Coefficients for evaluating Eqs. [2.12] through [2.15] with neutron energies between 5 and 20 MeV

	A	B	C	D
a	-0.000011493	138.80269	799.55938	-174.65853
b	0.00036556	1.16205	0.06663	9376.63316

c	-0.0031751	-0.0040091	-275.78493	-164341.05421
d	0.012203	-69.03516	-24762.65796	1002172.16358
e	0.20591			

2.4. Evaluation of f_{cpe} Verification/Validation

CPE is reached at the maximum recoil range of a proton for a specific incident neutron energy. NIST maintains the PSTAR database which provides data for stopping power and range of protons in ICRP tissue as a function of energy (NIST 2024). The resultant data (Figure 2-1) have been compared to the set of equations developed for this report.

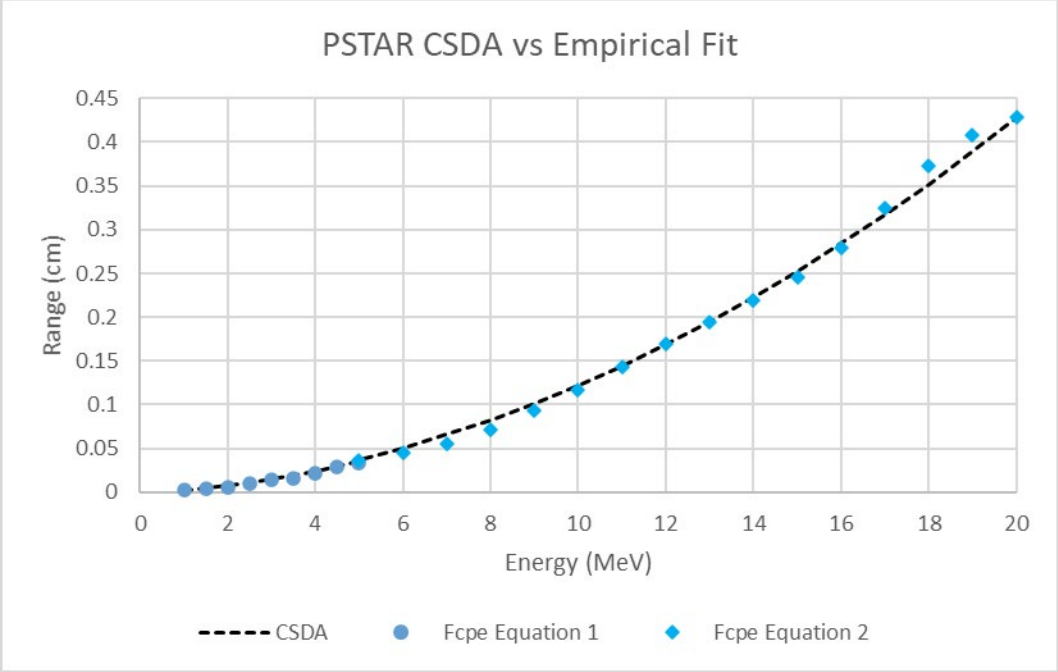

Figure 2-1. PSTAR versus Evaluated Data

Knowing that CPE is established at the maximum range of elastically scattered hydrogen, for each equation and energy the point at which CPE occurs is compared to PSTAR values by NIST (2024). Both empirically derived equations follow a similar trend to the continuous slowing down approximation (CSDA) in ICRU tissue (1989). There are slight discrepancies at several points, however, the functions developed still reflect results from probabilistic simulations.

As depicted in Figure 2-2, the equation is a good fit for the MCNP data collected. Additionally, values pulled from Chen and Chilton (1979a; 1979b) further confirm the MCNP functional fits. At very small shallow depths, Chen and Chilton's f_{cpe} is nearly twice that of what was calculated in this report. These differences are due to the different tissue segment thicknesses simulated. Significant computational improvements since that time allow for reasonable simulation of tissue segments in the micron range. Chen and Chilton (1979a; 1979b) were limited to 1 mm segments of tissue slices and therefore their results are not as accurate.

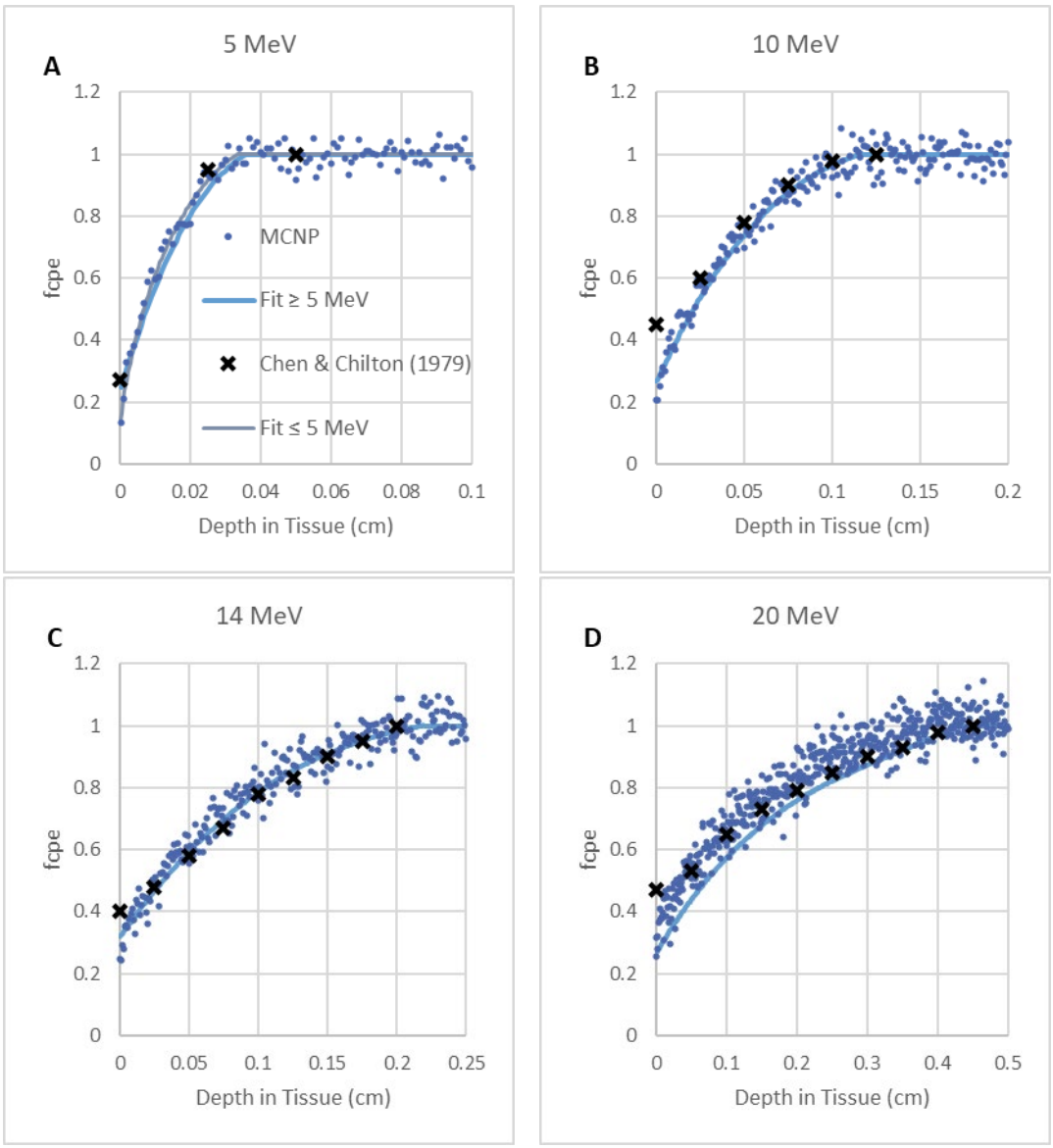

Figure 2-2. f_{cpe} Comparisons (a) 5 MeV (b) 10 MeV (c) 14 MeV (d) 20 MeV

2.5. Neutron Energy Degradation Model for Shielding

A first-principles, deterministic model for calculating the degradation in energy fluence of a beam of neutrons traversing a one-dimensional infinite (i.e., zero leakage) shield is used in the neutron dose module. This model is based on Fermi age theory (an extension of age-diffusion theory) to compute the probability of energy losses due to scattering events combined with neutron attenuation using the Beer-Lambert law.

The NeutronDose module computes energy flux attenuation using this new shielding energy-degradation model. In this model the incoming neutron energy spectrum is discretized into 40 bins and energy degradation is accounted for separately in each of those bins.

Neutron Energy Degradation. The neutron energy degradation model developed for use in VARSKIN+ is a deterministic, first-principles calculation intended to be used for estimating the effectiveness of various shielding materials at reducing the dose rate from neutrons. The consideration of energy dependence makes it more accurate than a simple removal-type attenuation scheme, but its energy spectrum calculation is not as accurate as Monte Carlo methods of neutron transport. VARSKIN+ allows the user to degrade neutrons through water shields with future upgrades to include other shielding materials generally of interest in neutron dosimetry.

The model addresses two types of interactions: slowing down (caused by scattering) and removal (caused by any reaction that is not scattering). Probabilities of the occurrence of each type of interaction are used to determine the proportion of neutrons that are entering and leaving a series of energy bins at a given depth in shielding. Determination of these probabilities is dependent on the cross section for each interaction, and the shield is thus defined in terms of its elemental composition.

GUI Updates. The neutron dose module GUI allows the user to define a shield, observe (in the form of the neutron spectrum graph) the energy degradation provided by the shield, and perform a side-by-side comparison of shielded and unshielded doses. Current capability is limited to water shields. Figure 2-3 shows the updated neutron module GUI which includes a “Shield” button next to the “Spectrum” button. Additionally, dose equivalent is provided for “Unshielded” and “Shielded” exposure scenarios.

Selecting the “Shield” button opens the dialog shown in Figure 2-4. The table starts out blank (no lines). New lines can be added with the “Add Line” button, and lines can be removed with the “Remove Line” button. Each line represents a new

shield. The line shown in the figure is the default, which will appear whenever “Add Line” is clicked. Clicking “Reset” will delete all lines from the table, disabling shielding. Clicking “Apply” will recalculate the neutron spectrum for the selected neutron source using the shield specified in the table. Either button will also close the dialog box.

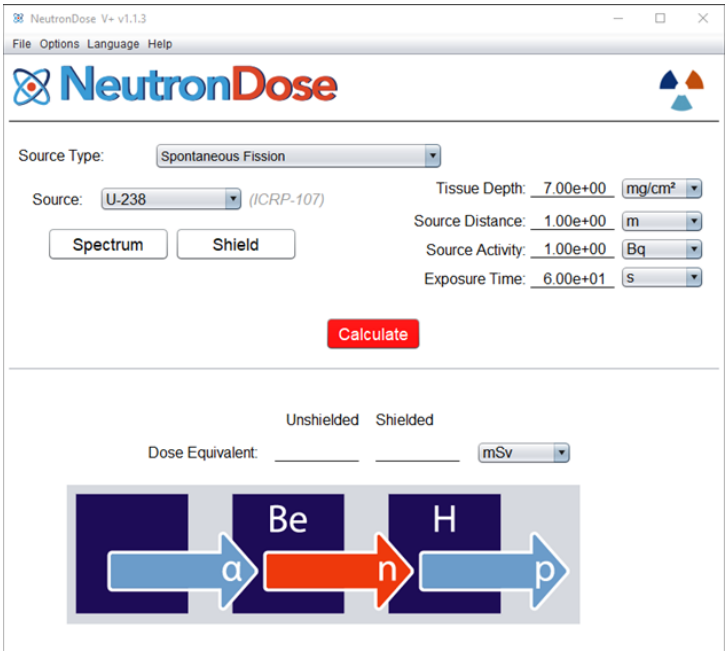

Figure 2-3. Updated neutron model screen.

Shields are specified as a list of “segments” from closest to the source (number 1) to closest to the receptor. The material composition of a shield segment is specified using a drop-down menu, which selects from preset compositions. Currently, only water is available in this list, as this is the only material specifically validated --- others will become available in later versions, and as more nuclides’ ENDF tapes can be reliably read. Density (in g/cm^3) and depth (in cm) are also required for defining a shielding segment; these units are not changeable by the user. The user may specify as many segments as desired.

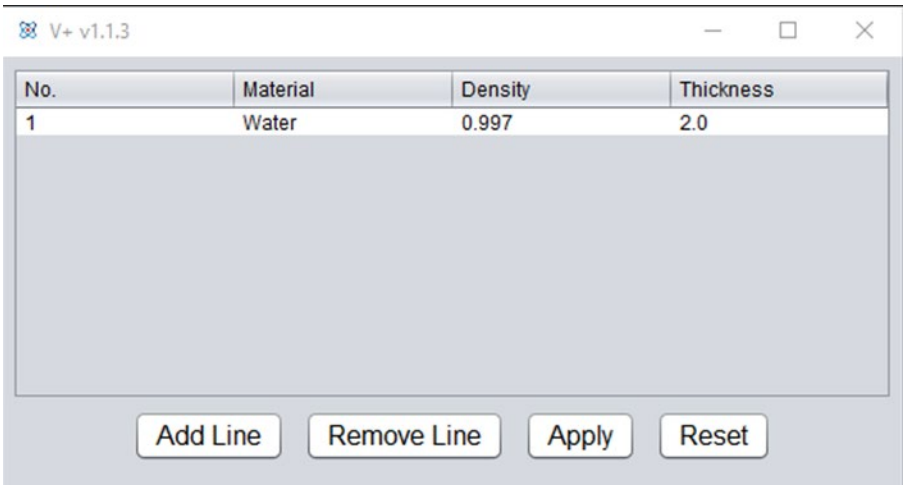

Figure 2-4. Neutron shield definition dialog.

Degraded energy flux is recalculated when the shield or source is updated. The problem geometry parameters on the right of the window in Figure 2-3 (i.e., tissue depth, source distance, source activity, and exposure time) do not affect the shielding calculation.

The Neutron Spectrum display appears when the user clicks the “Spectrum” button on the module screen. Two radio-type menu options allow the user to switch between unshielded and shielded spectra (Figure 2-5). If no shielding is specified, these menu options are grayed out and only the unshielded spectrum is displayed. The graph can be saved as a PNG file from this menu.

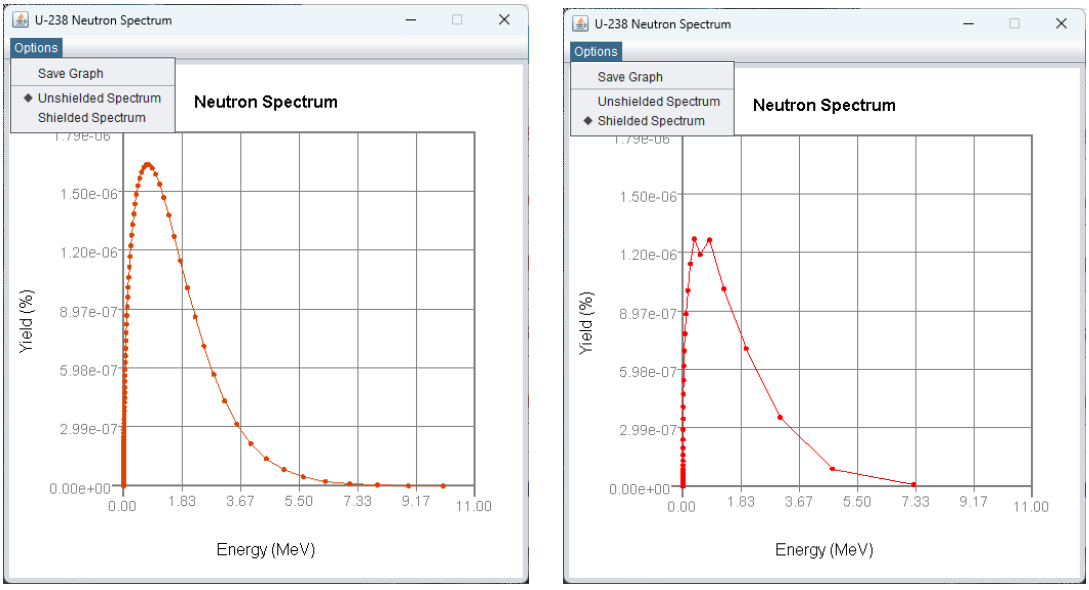

Figure 2-5. Neutron spectra for unshielded (left) and shielded (right) sources

Verification. Output of the neutron energy degradation model was verified by comparison to MCNP (LANL 2003) simulations with the same one-dimensional infinite assumptions used to produce the flux model described above. Specifically, the MCNP model comprised a sphere separated into "shells" of increasing radii. Neutrons were emitted by an isotropic point source at the center of the sphere. Neutron fluence was tallied at the surface of each shell and binned into the same 40 energy bins used by the VARSKIN+ neutron model. A cosine bin was also used to ensure that only "forward-moving" (i.e., not backscattered) neutrons were counted. To provide a straightforward comparison between the two models, the average neutron energy traversing each shell of the MCNP model was compared to the average neutron energy calculated by NeutronDose for an equivalent thickness of shielding.

The same method was used for both the MCNP results and V+ NeutronDose results to eliminate the potential for error caused by MCNP performing the energy-averaging operation differently. Error in the MCNP results is reported as the relative error, defined as the standard deviation divided by the estimated mean, for each energy bin in each tally.

The standard deviation must be extracted from the reported relative error as above and then propagated through the calculation to produce standard deviation of the average energy. Variance reduction was achieved using importance splitting for the various shells in accordance with a standard technique described in the MCNP 6.2 manual (Pelowitz et al. 2013). A sufficient thickness of material was included in the model to ensure that the farthest shell from the source (greatest radius) tallied zero neutron flux.

Results. The monoenergetic neutron sources selected for testing in MCNP are 16.735 MeV, 955 keV, and 1305 eV. These energies correspond to the centers of the energy bins that contain 20 MeV, 1 MeV, and 1 keV, respectively. As a result, these are the responses that the V+ neutron-energy model would have for neutrons of those (round) energies.

The average energy calculated by MCNP for various depths in water shielding is found to be in good agreement with the results from the V+ neutron model. Figure 2-6 to Figure 2-8 depict the average energy response for 16.735 MeV, 955 keV, and 1305 eV neutrons. The graphs are terminated at the depth where MCNP begins tallying zero neutron flux. Percent error for the high-energy graph is less than 20% at and below 16 cm. The 955 keV results are below 31% error until 4 cm, before increasing to 75% error by 10 cm. Error then remains below 95%. The low-energy results are within 26% at and below 4 cm, before increasing up to about 100% thereafter. At these greater depths with larger percent differences, most of

the neutron energy and neutron dose have already been delivered to shallower layers.

With very few exceptions, the relative error reported by MCNP for each tally is less than 0.1, i.e., the threshold specified for a reliable tally. Standard deviation for the calculated average energy values are two (or more) orders of magnitude less than the average energy values, and so error bars are omitted from the graphs (too small to visualize).

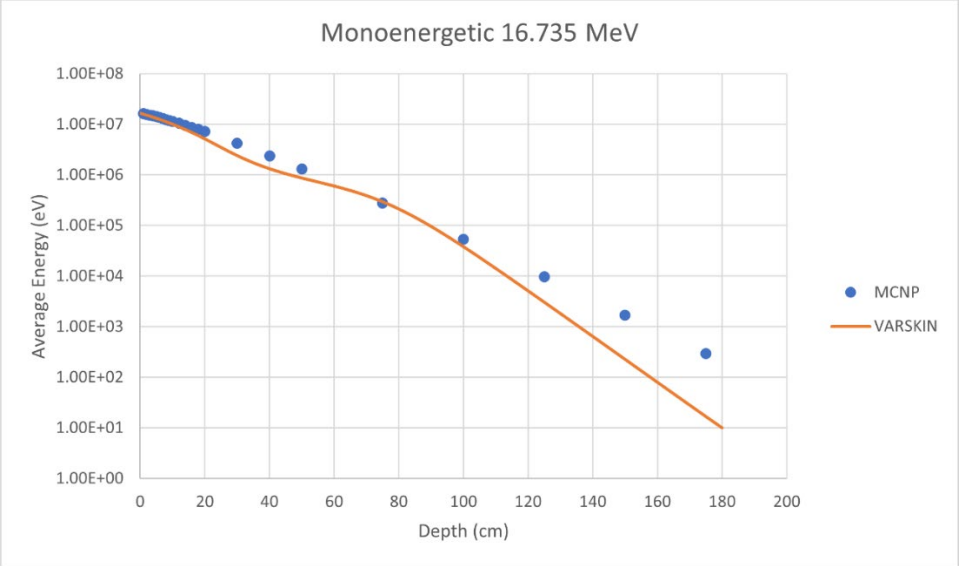

Figure 2-6. Average energy response for 16.735 MeV neutrons.

In general, the V+ neutron energy model displays the proper behavior while generally underpredicting the energy returned by MCNP. The percent error metric is somewhat misleading, especially for the 1305 eV test, because after a certain point the V+ model will "flatline" at 0.211 eV while MCNP's average energy continues to drop. This appears to cause a very large percent error (upwards of 500%), but this is the result of the V+ routine being incapable of modeling, with high fidelity, neutron energy degradation below 1 eV.

Because of the manner in which V+ treats thermal neutrons, V+ will tend to overpredict dose for neutrons that are thermalized at higher than room temperature, i.e., the thermal average cross sections calculated for the lower temperature will be greater than those calculated at the correct, higher temperature. By a similar argument, V+ will tend to underpredict dose for neutrons that are thermalized at less than room temperature.

The higher percent errors at other points in the 955 keV and 1305 eV graphs are attributed to the smaller overall values on those graphs. For example, the 26% error on the 1305 eV graph occurs where the absolute error is only 6 eV.

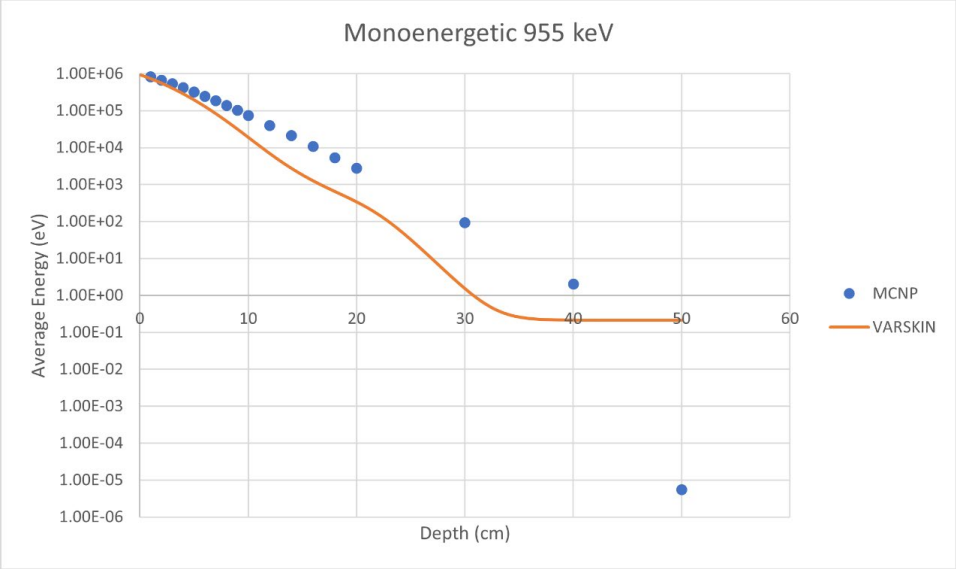

Figure 2-7. Average energy response for 955 keV neutrons.

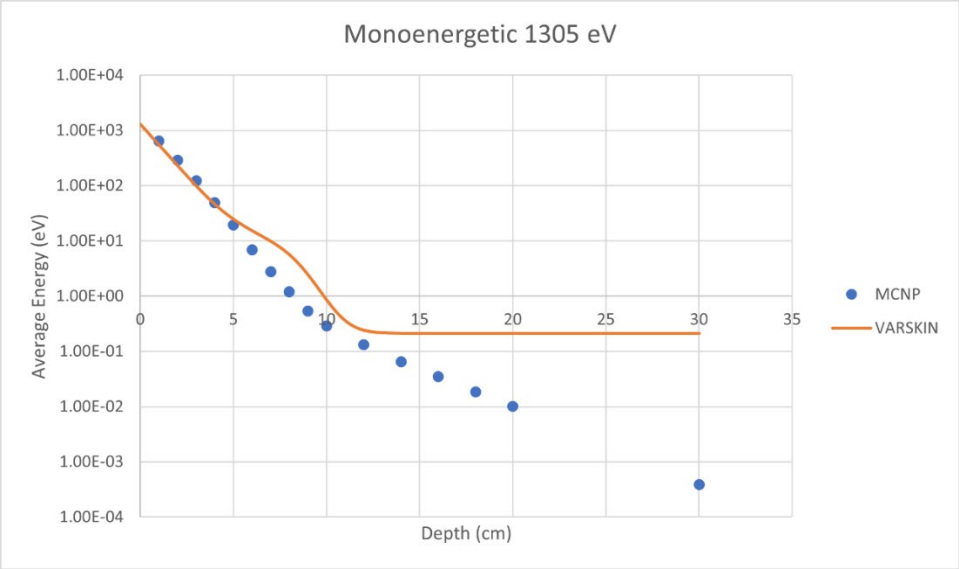

Figure 2-8. Average energy response for 1305 eV neutrons.

2.6. Evaluation of KERMA

Pertinent cross sections were gathered from the Evaluated Nuclear Data File (ENDF) to build neutron KERMA in tissue (LANL 2024). Each of the possible neutron reactions was evaluated individually before summation to determine the total KERMA per unit fluence at a given incident neutron energy (Figure 2-9). Comparisons with ICRU 63 (2001) and (Lui and Chen 2008) are provided.

(a)

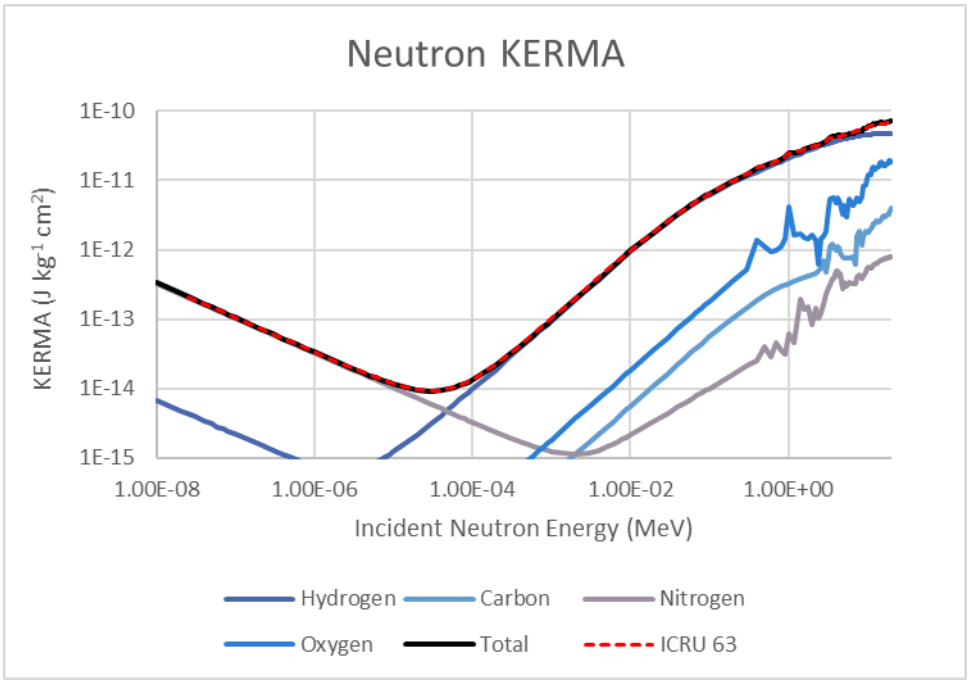

(b)

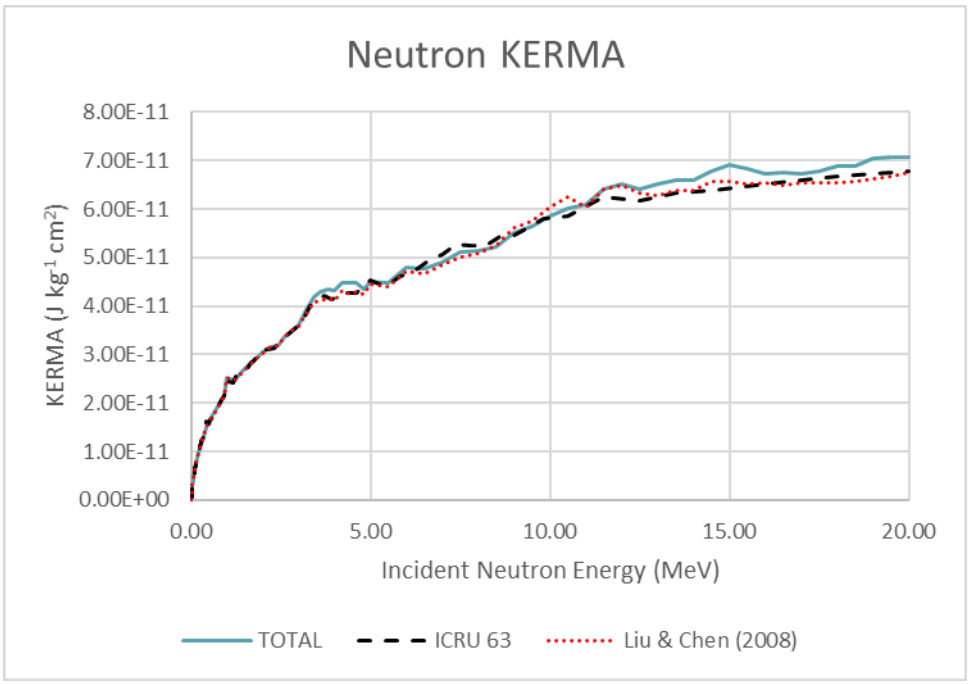

Figure 2-9. (a) Neutron KERMA per unit fluence as a funtion of energy and element for low-energy neutrons; (b) Neutron KERMA per unit fluence versus energy for high-energy neutrons.

The evaluated data compare well with the ICRU (2001) values. However, there are variations in the higher MeV range primarily because of the modeling of

threshold reactions in oxygen, nitrogen, and carbon. A previous study conducted by Liu and Chen (2008) evaluated the constituent KERMA extensively and reported a new set of values. Their results are compared in Figure 2-10 to the evaluated data from Anspach (2020) and ICRU recommendations.

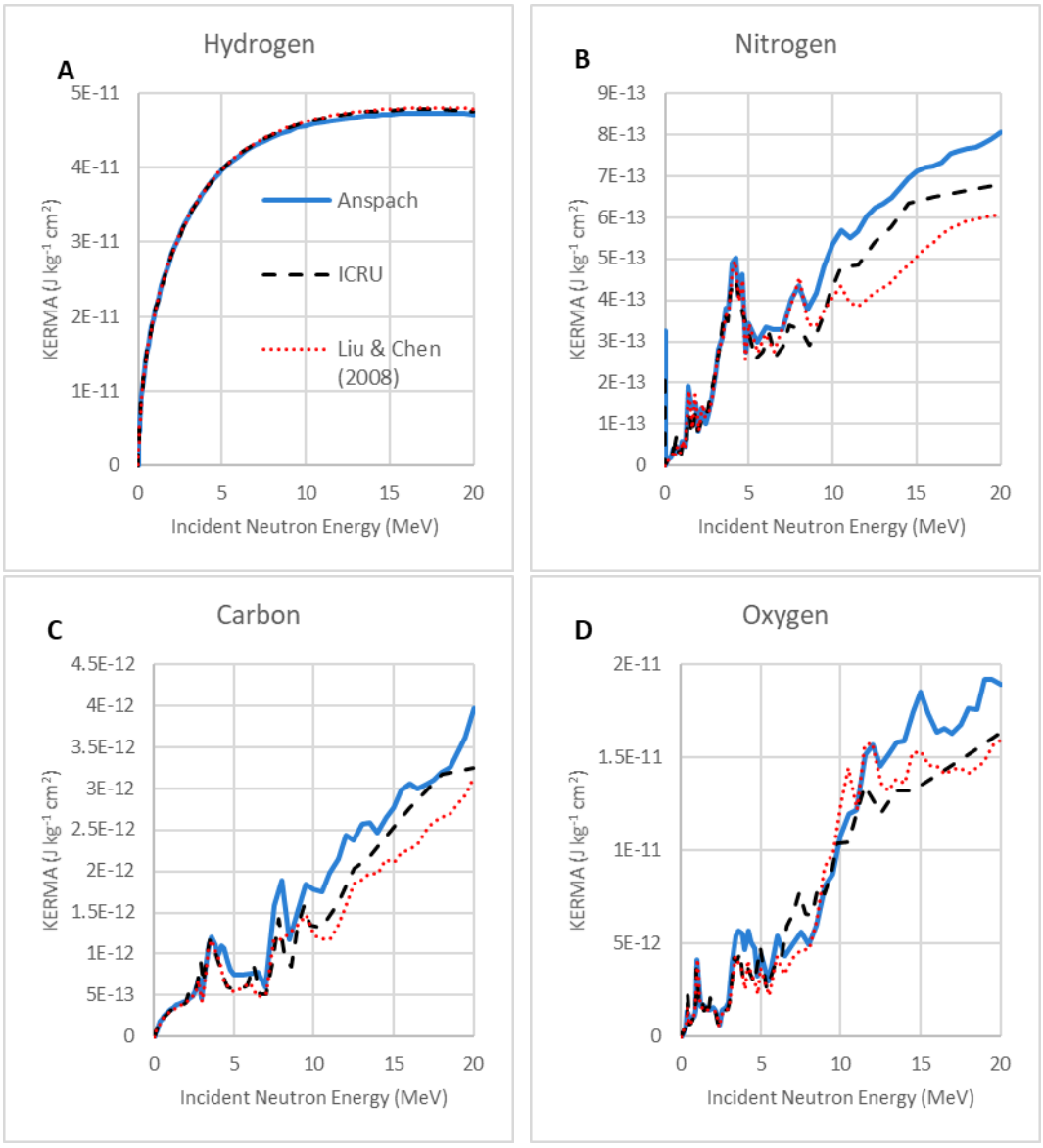

Figure 2-10. Threshold Reactions in each of the Four Constituents Accounted for in KERMA as a Function of Incident Neutron Energy

Using ICRU 63 (2001), “Nuclear Data for Neutron and Proton Radiotherapy and for Radiation Protection” for comparison, the recent difference for the reported KERMA values is determined over the entire energy range modeled as shown in Figure 2-11. Generally, there are three ranges with noticeable variations in their

trends. This includes the energy ranges of $1x10^{-8}$ to $1x10^{-5}$ MeV, $1x10^{-5}$ to $1x10^{-2}$ MeV, and $1x10^{-2}$ to 20 MeV.

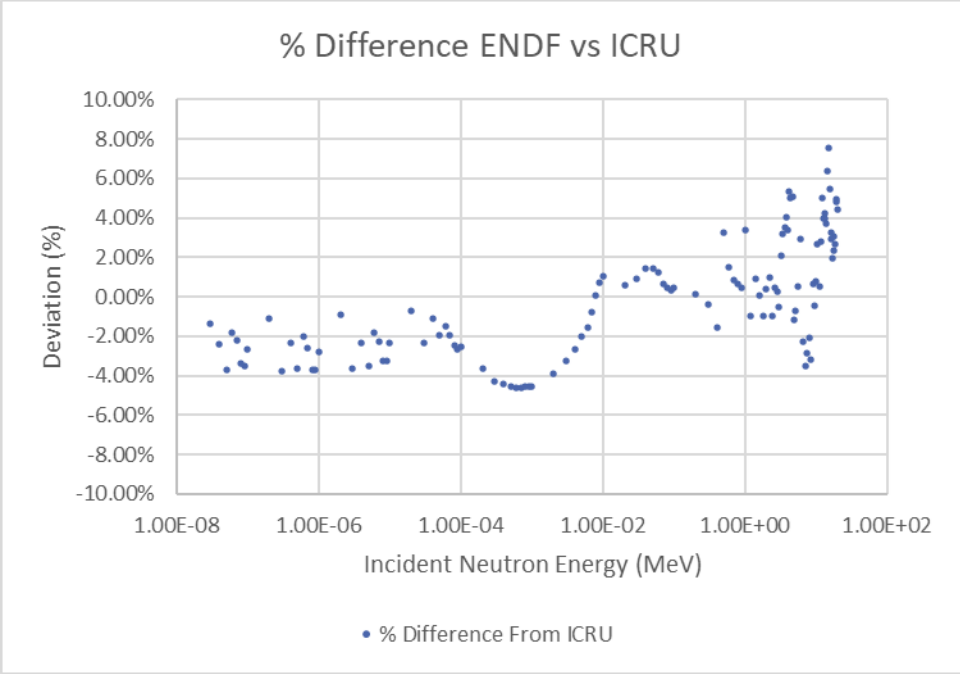

Figure 2-11. Percent Difference Between Neutron Dose using ENDF Files (2024) versus ICRU 63 (2001)

In the first energy range (Figure 2-12), the reaction that represents nearly the entire KERMA is the $^{14}N(n,p)^{14}C$ reaction with some fraction of the total KERMA due to radiative capture with hydrogen and other elemental constituents. Generally, the methods used here are in strong agreement (within 2 to 4 percent) with ICRU 63 (2001) in this energy range.

As energy increases (Figure 2-13), the probability of these reactions declines. In the energy range from $1x10^{-5}$ to $1x10^{-2}$ MeV, the probability for elastic scatter dramatically increases such that the dominant reaction mechanism is elastic scatter with hydrogen. Resultant data are still in good agreement with ICRU 63 (2001). The transition, however, between these two reactions is a well-documented physical phenomenon such that any variation between methods will be represented systematically in the percent difference plot.

Above 0.01 MeV (Figure 2-14), inelastic scatter and transfer reactions constitute a significant portion of total KERMA. Variation in this region is primarily due to the different cross-sectional data referenced. Published in 2000, the KERMA values of ICRU 63 (2001) are based on the ENDF/B-V1.0 evaluated cross sectional data. In this report, cross section data from ENDF/B-VIII.0 (2018) are accessed. Figure 2-14 demonstrates the complexity of neutron KERMA in this energy range.

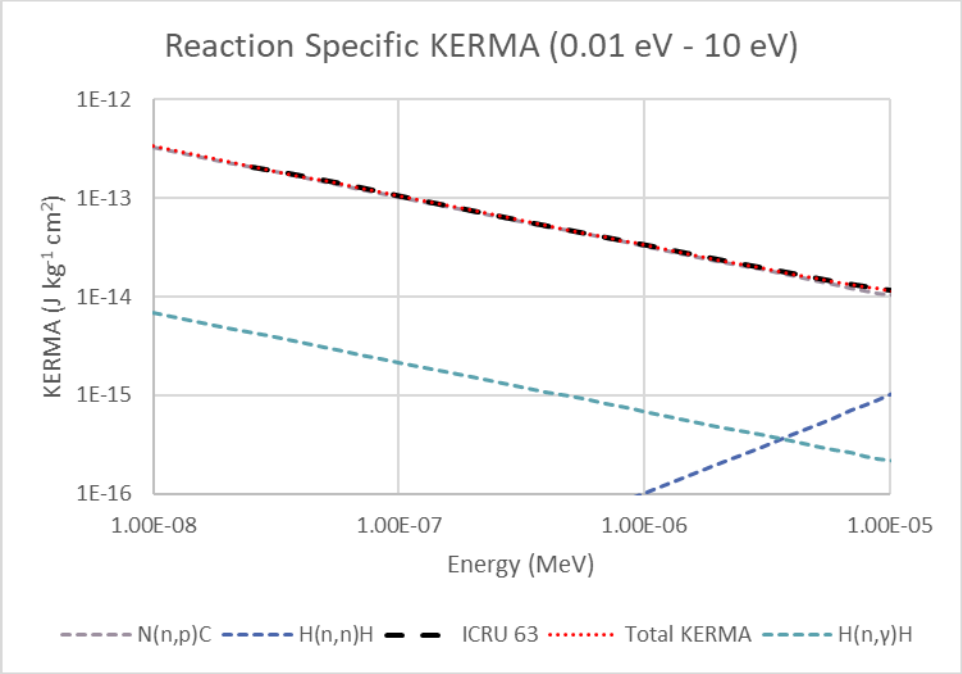

Figure 2-12. Reaction-Dependent KERMA in the Thermal Energy Range

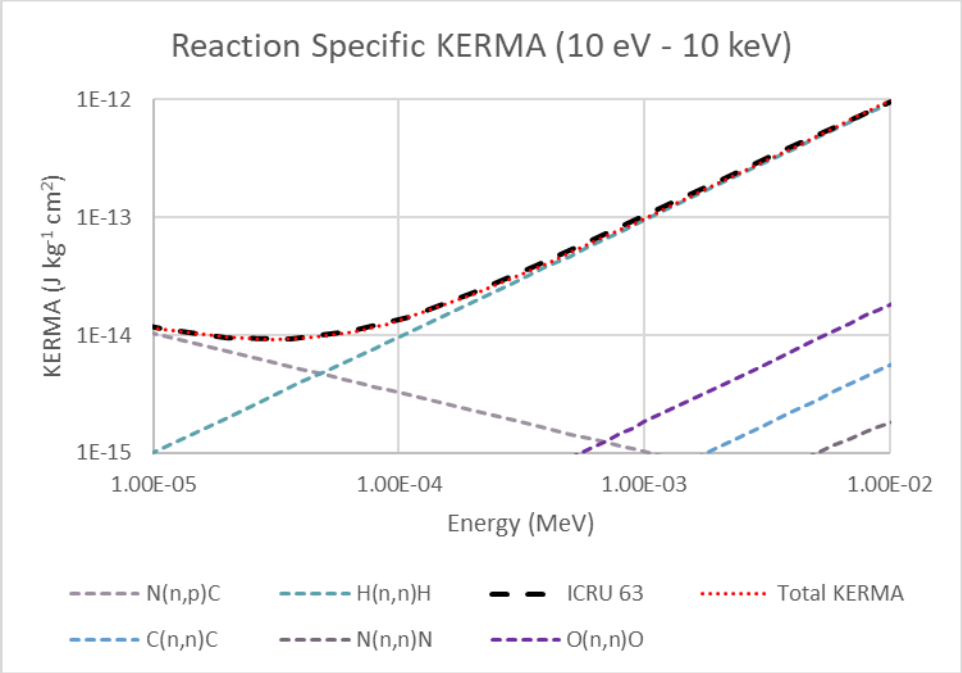

Figure 2-13. Reaction-Dependent KERMA in the Intermediate Energy Range

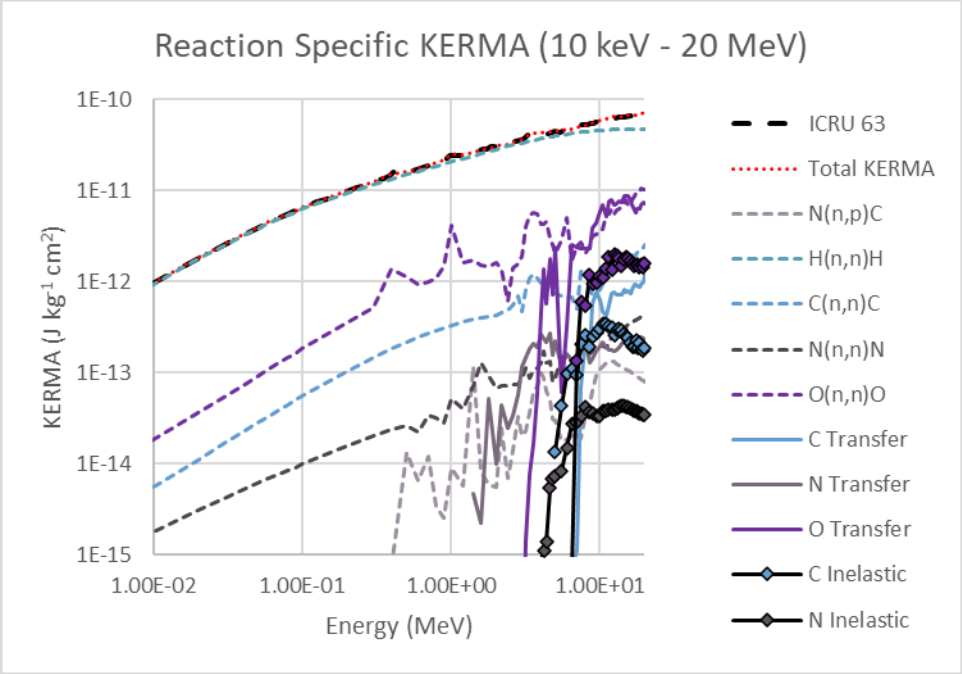

Figure 2-14. Reaction-Dependent KERMA in the Fast Energy Range

2.7. Neutron Dose from Radiative Capture

Whenever a nucleus enters an excited state, it has a high probability of emitting gamma rays to return to its ground state. In radiative capture, inelastic scatter, and transfer reactions, gamma rays are produced and will ultimately impart energy. However, unlike charged particles, they may travel significant distances before interacting with the medium or leaving it entirely.

For small critical volumes, such as that where the shallow dose estimates are made, generated photons have a very small interaction probability. For larger volumes, such as the whole body, the interaction probability increases necessitating the determination of photon dose. This is especially important for thermal neutrons where the $^{1}H(n,\gamma)^{2}H$ capture reaction prevails.

Concepts employed in internal dosimetry can be adopted to approximate photon dose. Since capture reactions within the human are a probabilistic occurrence, the production of photons is assumed to be randomly distributed throughout the entire body of the exposed. This concept is similar to a homogeneously distributed radionuclide that emits photons during radioactive decay. In this case, the number of photons produced per unit mass of a neutron-generated distributed gamma emitter is given by Eq. [2.16]:

$$\gamma \left[\frac{photons}{kg}\right] = \Phi \, N_j \, \sigma_{ij} \qquad [2.16]$$

where Φ is the neutron fluence, N_j is the number of atoms per unit mass of a specific constituent, and σ_{ij} is the cross section of that specific reaction leading to the production of photons. Photon production from Eq [2.14] is converted to dose by Eq. [2.17]:

$$D_\gamma = \gamma \, F_a \, E_\gamma \, k \qquad [2.17]$$

where F_a is the absorbed fraction to the whole body from a photon of energy, E_γ, and *k* is a unit conversion factor. Summing doses for all photon production reactions yields the total whole-body photon dose.

ICRP 23 (1975), "Reference Man: Anatomical, Physiological, and Metabolic Characteristics" reports a series of Monte-Carlo tests that determined the fraction of energy absorbed by a target organ from a photon of a specific energy emitted in a source organ. Figure 2-15 depicts the whole-body absorbed fraction, as a function of photon energy, from a homogeneously distributed whole-body source.

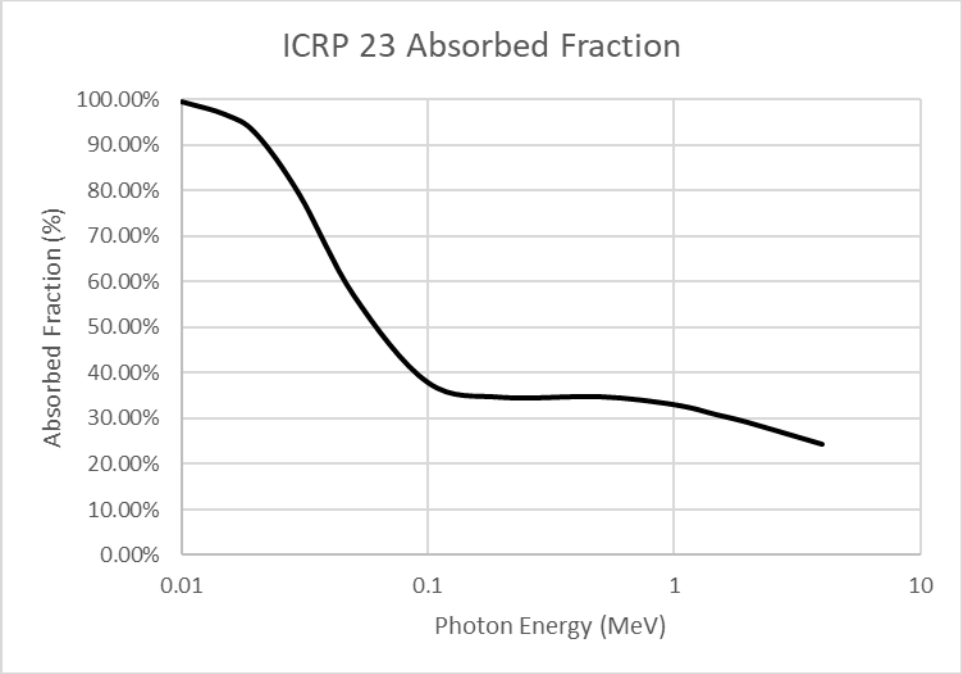

Figure 2-15. ICRP 23 (1975) Absorbed Fraction of Photon Energy Emitted from the Body and Absorbed in the Body

This process is separate from shallow neutron dosimetry where the assumption of charged particle equilibrium is not valid for fast neutrons. In this case, local energy deposition in small tissue volumes is the primary concern for neutron dose. Photons generated in these small critical volumes have a very low probability of interaction and are assumed to leave the critical target in its entirety. However, for whole body dosimetry where the tissue volume is many orders of magnitude larger than a 10-micron tissue segment, photon dose must be considered.

Below energies of about 10^{-5} MeV whole body radiation photon dose is nearly one order of magnitude larger than the neutron dose (Figure 2-16). This is primarily due to the relatively large hydrogen capture cross section. This photon effect steady decreases with increasing neutron energy until approximately 0.5 MeV, where threshold inelastic and transfer reactions begin to occur. At neutron energies above about 2 MeV, the contribution to total dose from photons—primarily generated from inelastic scattering of neutrons—begins to climb until about 10 MeV where it is approximately an order of magnitude less than the contribution from neutrons.

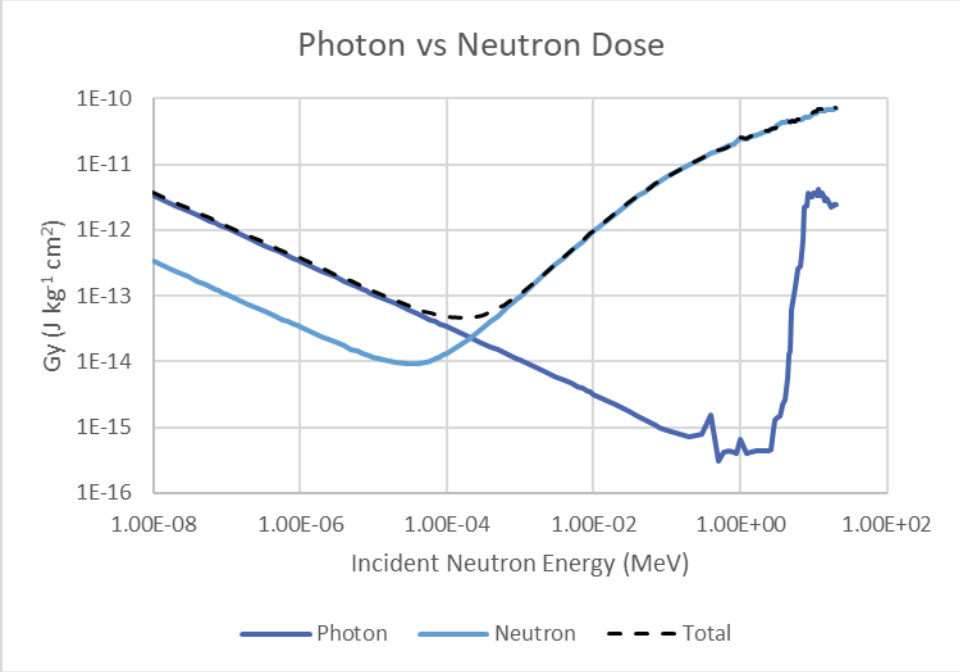

Figure 2-16. Absorbed Dose Due to Neutrons and Photons as a Function of Incident Neutron Energy

For neutron dose from radiative capture, whole body dosimetry is calculated by Eq. [2.18]:

$$H(E) = D_{\gamma}(E) \cdot w_{R\gamma} + H_n(E) \qquad [2.18]$$

where $D_\gamma(E)$ is the absorbed dose from all photons produced from nuclear reactions associated with a specific neutron energy and $w_{R\gamma}$ is equal to unity (1), the radiation weighting factor for photons. The equivalent dose due to neutrons, $H_n(E)$ is described by the general neutron dosimetry model of NeutronDose, assigning fractional CPE a value of one, as CPE is assumed to be established.

3.0 REFERENCES

Anderson, M.E. and R.A. Neff. Neutron energy spectra of different size ^{239}Pu-Be(α,n) sources. *Nucl. Instrum. Methods.* 99: 231-235. 1972.

Anspach, L.J. Development of a fundamental depth-dependent neutron dosimetry model. Master's Thesis. *Oregon State University*. Corvallis, OR: 2020.

Chen, S.Y. and A.B. Chilton. Depth-Dose Relationship near the Skin Resulting from Parallel Beams of Fast Neutrons. *Radiation Research*. 77(1): 21-33. 1979a.

Chen, S.Y. and A.B. Chilton. Calculation of Fast Neutron Depth-Dose in the ICRU Standard Tissue Phantom and the Derivation of Neutron Fluence-to-Dose-Index Conversion Factors. *Radiation Research*. 78(3): 335-370. 1979b.

Hamby, D.M.; Mangini, C.D.; Luitjens, J.M.; Boozer, D.L.; Tucker, Z.G.; Rose, C.T.; Flora, R.S. VARSKIN+ 1.0: A Computer Code for Skin Contamination and Dosimetry Assessments. U.S. Nuclear Regulatory Commission. NUREG/CR-6918, Rev 4. July 2021.

International Commission on Radiological Protection (ICRP). "Reference Man: Anatomical, Physiological, and Metabolic Characteristics." Publication 23. Oxford, England: Pergamon Press. 1975.

International Commission on Radiation Protection (ICRP). "Nuclear Decay Data for Dosimetric Calculations." Publication 107. Ann. ICRP 38 (3). 2008

International Commission on Radiation Units and Measurements (ICRU). "Tissue Substitutes in Radiation Dosimetry and Measurement." ICRU Report 44. Bethesda, MD: International Commission on Radiation Units and Measurements. 1989.

International Commission on Radiation Units and Measurements (ICRU). "Nuclear Data for Neutron and Proton Radiotherapy and for Radiation Protection." ICRU Report 63. Bethesda, MD: International Commission on Radiation Units and Measurements. 2001.

Los Alamos National Laboratory (LANL). https://t2.lanl.gov/nis/data/endf/ last accessed November 2024.

Liu, Z. and J. Chen. New Calculations of Neutron Kerma Coefficients and Dose Equivalent. Journal of Radiological Protection, 28, 185-193. 2008.

Lorch, E.A. Neutron spectra of ^{241}Am/B, ^{241}Am/Be, ^{241}Am/Fe, ^{242}Cm, ^{239}Pu/^{13}C and ^{252}Cf isotopic neutron source. *J. Appl. Radiat. Isot.* 24:585-591. 1973.

Los Alamos National Laboratory, X-5 Monte Carlo Team. "MCNP—A General Monte Carlo N-Particle Transport Code, Version 5. LA-CP-03-0245. Los Alamos, NM: LANL. 2003.

Pelowitz, D.B.; Goorley, J.T.; James, M.R.; et al. MCNP6 User's Manual. Los Alamos National Laboratory. Technical Report No. LA-CP-13-00634. Los Alamos, NM: May 2013.

National Nuclear Data Center. ENDF/B-VIII.0 Evaluated Nuclear Reaction Data Library. February 2, 2018. https://www.nndc.bnl.gov/endf-b8.0/ last accessed December 2024.

https://physics.nist.gov/PhysRefData/Star/Text/PSTAR.html last accessed November 2024.

Shultis, J.K. and Faw, R.E. Radiation Shielding. American Nuclear Society. ISBN 0-89448-4567. La Grange Park, IL. 2000.

U.S. Nuclear Regulatory Commission. Traub, R.J., W.D. Reece, R.I. Scherpelz, and L.A. Sigalla. "Dose Calculation for Contamination of the Skin Using the Computer Code VARSKIN." NUREG/CR–4418. Washington, DC: NRC. 1987.

U.S. Nuclear Regulatory Commission. Reece, W.D., S.D. Miller, and J.S. Durham. "SADDE (Scaled Absorbed Dose Distribution Evaluator), A Code to Generate Input for VARSKIN." NUREG/CR–5276. Washington, DC: NRC. 1989.

U.S. Nuclear Regulatory Commission. Durham, J.S. "VARSKIN Mod 2 and SADDE Mod 2: Computer Codes for Assessing Skin Dose from Skin Contamination." NUREG/CR-5873, PNL-7913. Washington, DC: NRC. 1992.

U.S. Nuclear Regulatory Commission. Durham, J.S. "VARSKIN 3: A Computer Code for Assessing Skin Dose from Skin Contamination." NUREG/CR-6918. Washington, DC: U.S. Nuclear Regulatory Commission. 2006.

U.S. Nuclear Regulatory Commission. Hamby, D.M., Lodwick, C.J., Palmer, T.S., Reese, S.R., Higley, K.A. "VARSKIN 4: A Computer Code for Skin Contamination Dosimetry." NUREG/CR-6918, Rev 1. Washington, DC: U.S. Nuclear Regulatory Commission. 2011.

U.S. Nuclear Regulatory Commission. Hamby, D.M., Mangini, C.D., Caffrey, J.A., Tang, M. "VARSKIN 5: A Computer Code for Skin Contamination Dosimetry."

NUREG/CR-6918, Rev 2. Washington, DC: U.S. Nuclear Regulatory Commission. 2014.

U.S. Nuclear Regulatory Commission. Hamby, D.M., Mangini, C.D. "VARSKIN 6: A Computer Code for Skin Contamination Dosimetry." NUREG/CR-6918, Rev 3. Washington, DC: U.S. Nuclear Regulatory Commission. 2018.

Walsh, R.L. Spin-dependent calculations of fission neutron spectra and fission spectrum integrals for six fissioning systems. *Nuc. Sci. Eng.* 102:119-133. 1989.